Electronic Supplementary Information

Preparation of mesoporous nitrogen-doped titania comprising large crystallites with low thermal conductivity

Yuta Shimasaki,[a] Takamichi Matsuno,[a] Quansheng Guo,[b] Atsushi Shimojima,[ac] Hiroaki Wada,[ac] Takao Mori[bd] and Kazuyuki Kuroda*[ac]

[a] *Department of Applied Chemistry, School of Advanced Science and Engineering, Waseda University, 3-4-1 Okubo, Shinjuku-ku, Tokyo 169-8555, Japan*

[b] *International Center for Materials Nanoarchitectonics (WPI-MANA), National Institute for Materials Science (NIMS), 1-1 Namiki, Tsukuba, Ibaraki 305-0044, Japan*

[c] *Kagami Memorial Research Institute for Materials Science and Technology, Waseda University, 2-8-26 Nishiwaseda, Shinjuku-ku, Tokyo 169-0051, Japan*
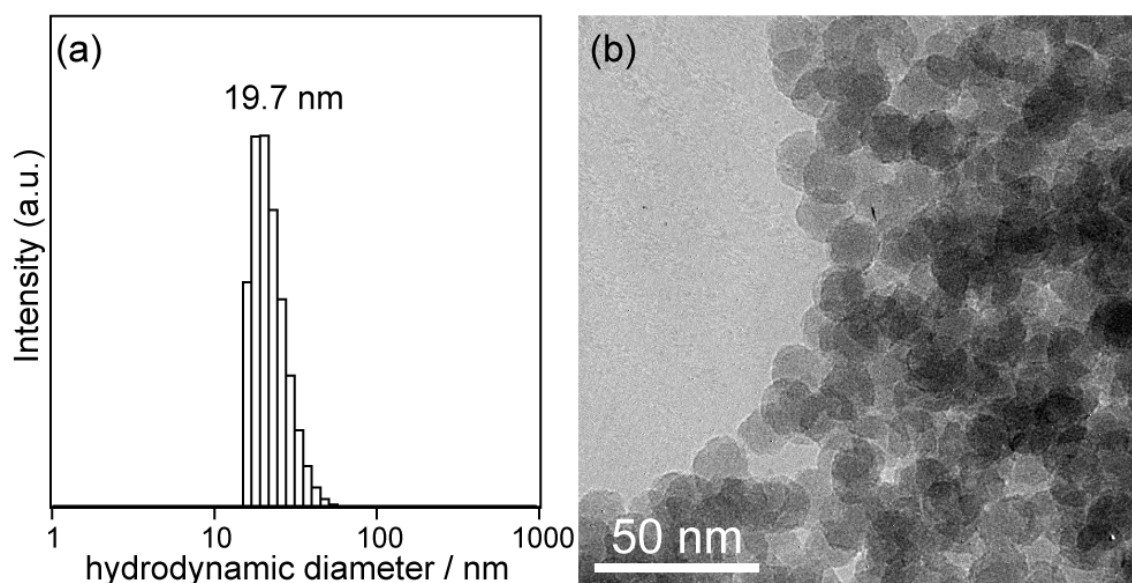
[d] *Graduate School of Pure and Applied Sciences, University of Tsukuba, 1-1-1 Tennodai, Tsukuba, Ibaraki 305-8577, Japan*
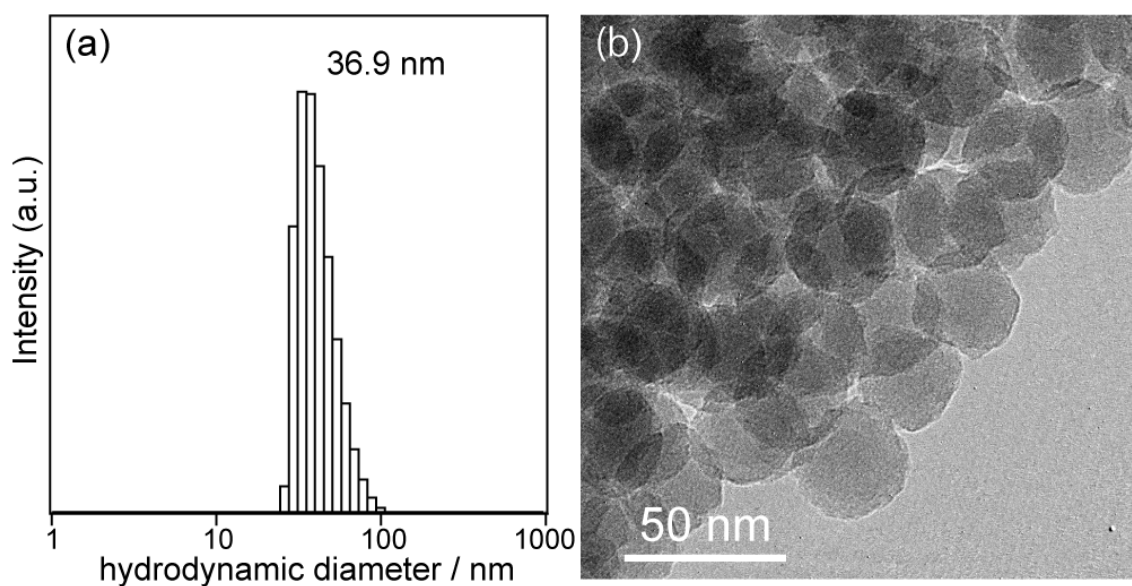
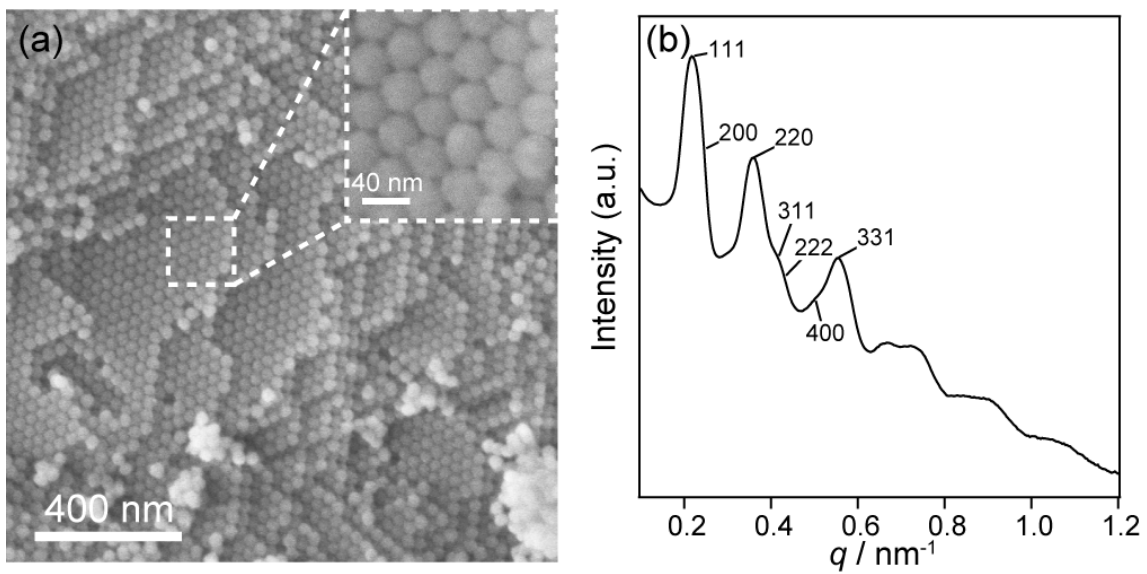Corresponding Author
E-mail: kuroda@waseda.jp

Table of contents

Fig. S1 (a) DLS profile and (b) TEM image of colloidal silica nanoparticles. The diameter is approximately 19 nm on the basis of these data.

Fig. S2 (a) DLS profile and (b) TEM image of colloidal silica nanoparticles. The diameter is approximately 35 nm on the basis of these data.

Fig. S3 (a) SEM images (inset: high-magnification) and (b) SAXS pattern of Ti-SCC.

Fig. S4 N_2 adsorption-desorption isotherms of Ti-SCC.
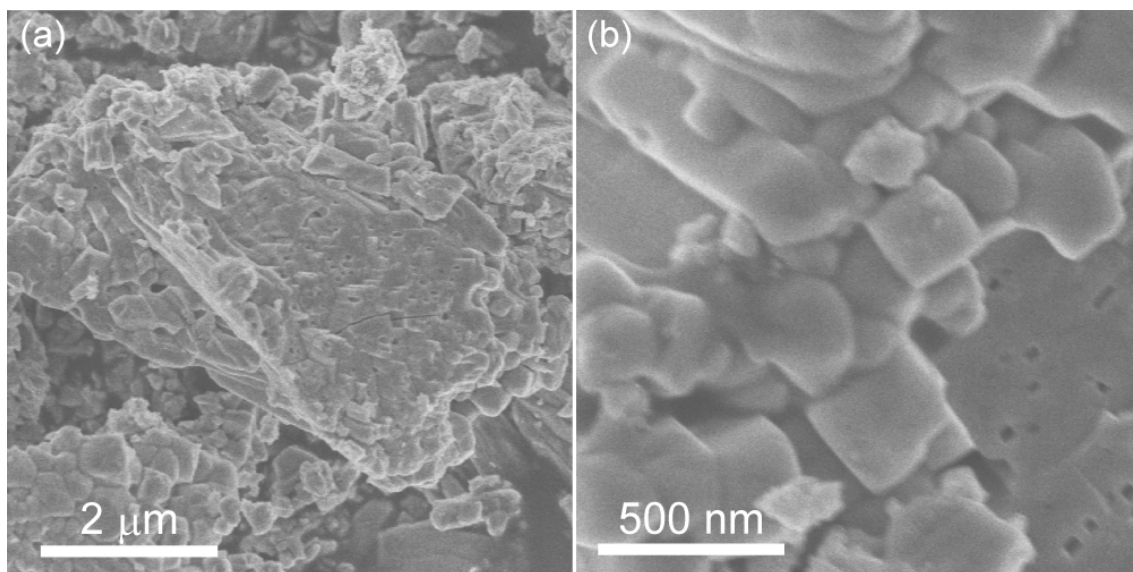
Fig. S5 SEM images of the pellet of meso N-TiO$_2$ sintered at 1073 K.
The mesostructures collapsed by the sintering above 873 K.
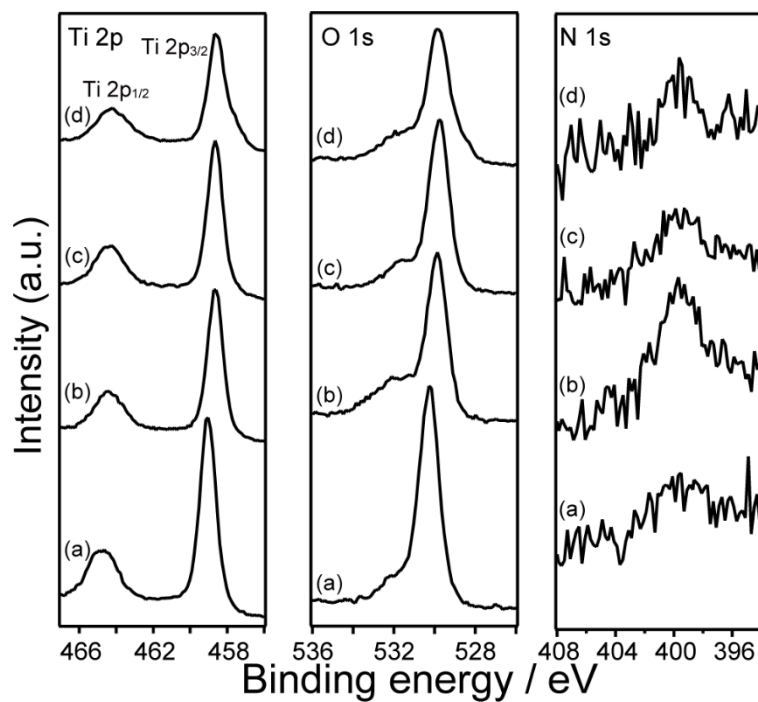
Fig. S6 XPS spectra of (a) template free-TiO$_2$, (b) template free-N-TiO$_2$, (c) template free-N-TiO$_2$_873, and (d) template free-N-TiO$_2$_1173: (left) Ti 2p, (center) O 1s, (right) N 1s.
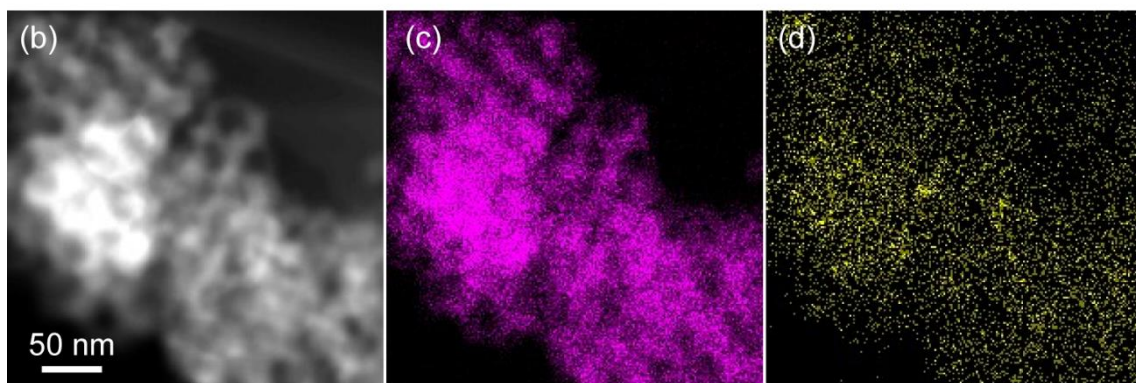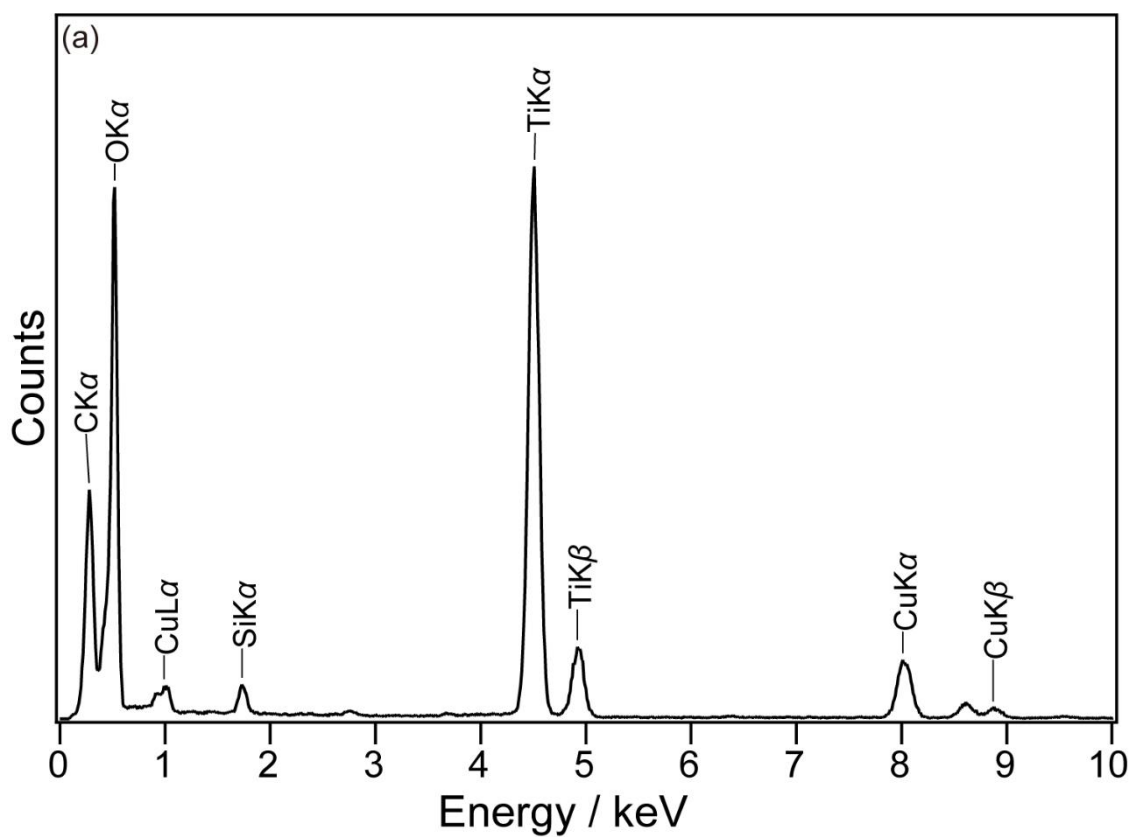
Fig. S7 (a) EDX spectrum, (b) BF-STEM image, and the corresponding EDX mapping of (c) Ti and (d) Si observed for meso-N-TiO$_2$. C and Cu were derived from the carbon-coated microgrids.
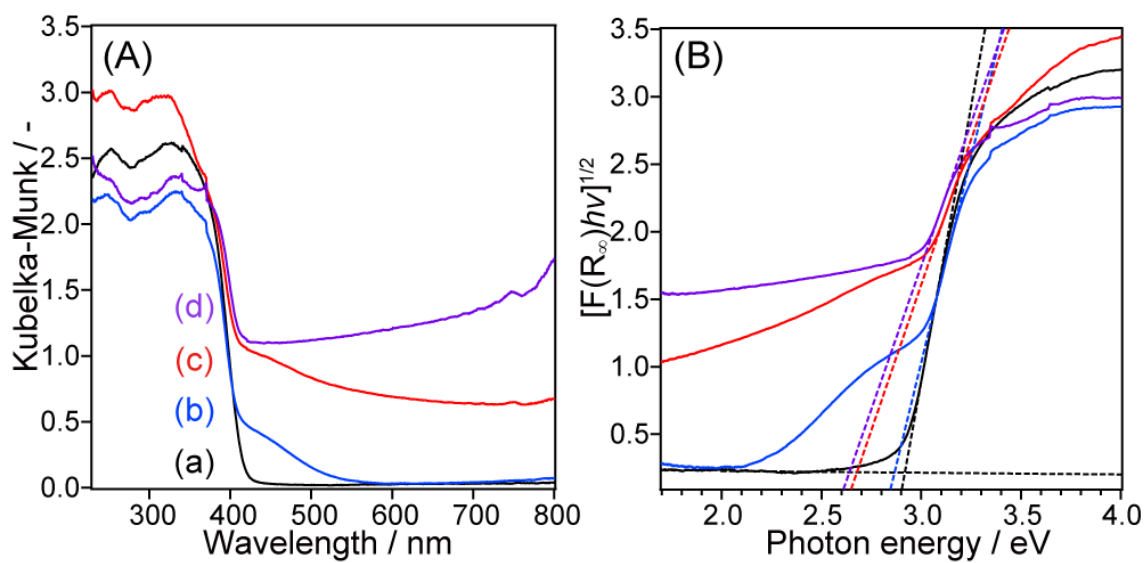
Fig. S8 (A) UV-vis DRS profiles and (B) Tauc plots of (a) template free-TiO$_2$, (b) template free-N-TiO$_2$, (c) template free-N-TiO$_2$_873, and (d) template free-N-TiO$_2$_1173.

(a) window pore

mesopore replicated from
silica nanoparticle

50 nm

(b) 0.32 nm

10 nm
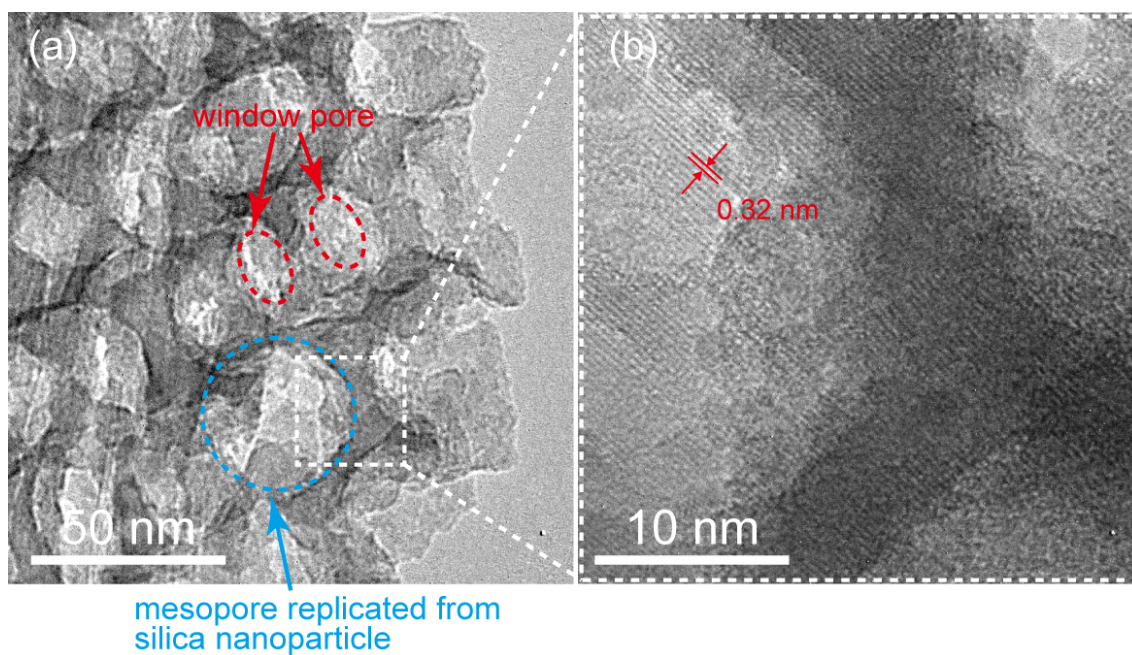
Fig. S9 High-magnification TEM images of meso-N-TiO$_2$.

(a) Blue dotted circle indicates a mesopore replicated from a silica nanoparticle. Red dotted circle indicates window pores. (b) The lattice fringe spacing was 0.32 nm and it was assigned to the (110) plane of rutile TiO$_2$.
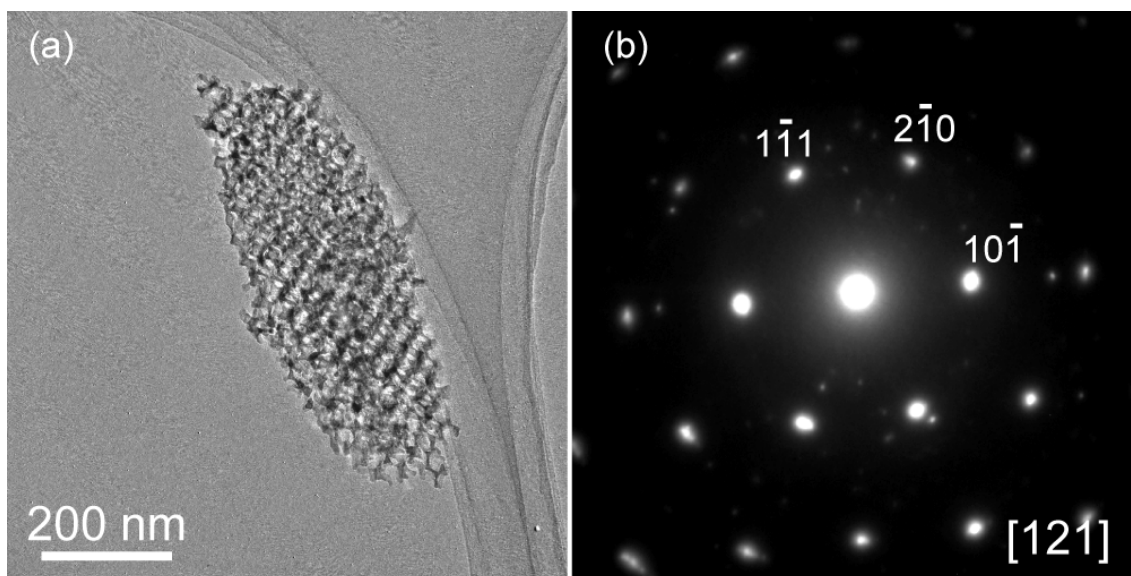
Fig. S10 (a) TEM image and (b) the SAED pattern of meso-TiO$_2$.
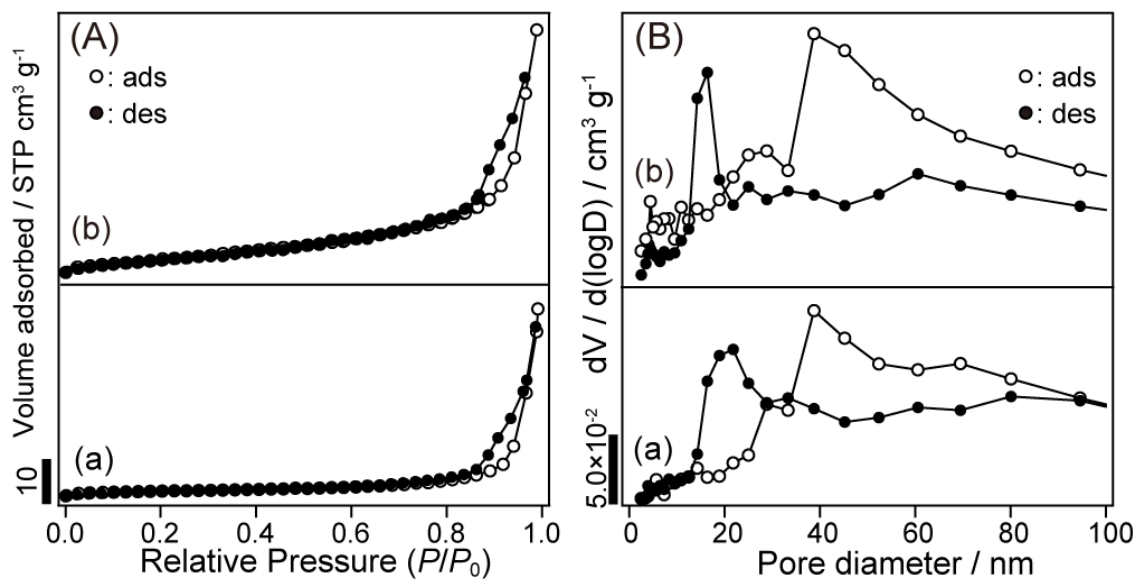
Fig. S11 (A) N$_2$ adsorption-desorption isotherms and (B) BJH pore size distributions of (a) meso-N-TiO$_2$ and (b) meso-N-TiO$_2$_873.
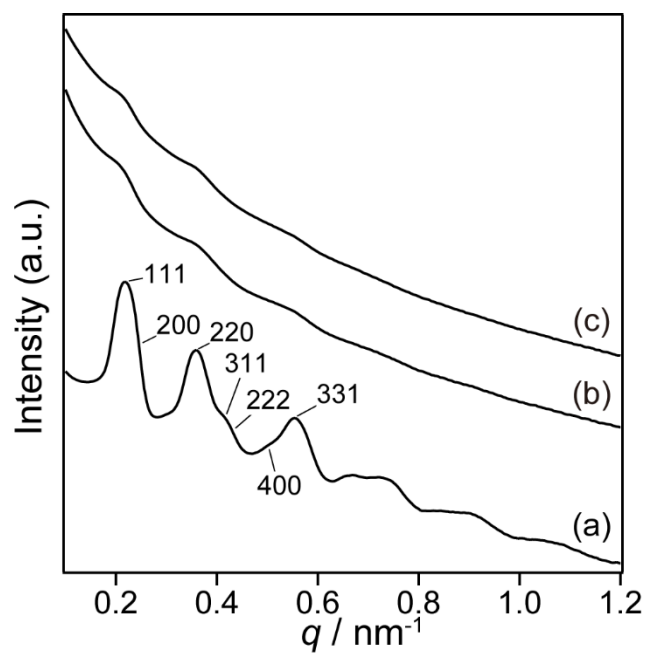
Fig. S12 SAXS patterns of (a) Ti-SCC, (b) meso-N-TiO$_2$, and (c) meso-N-TiO$_2$_873.
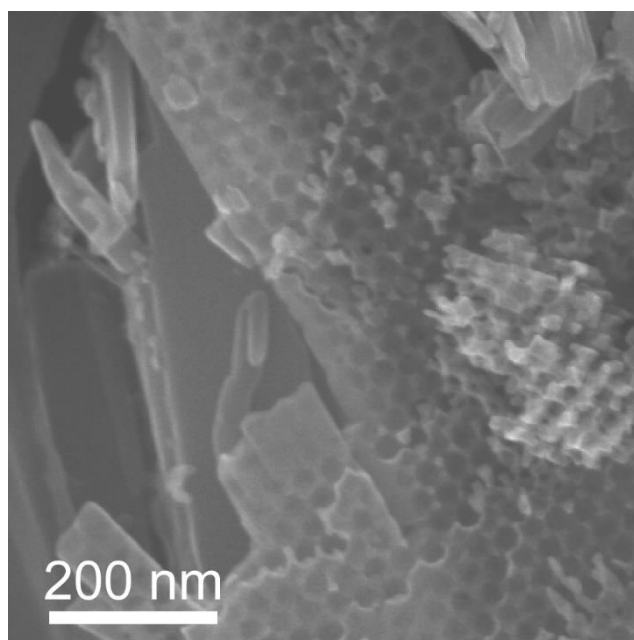
Fig. S13 SEM image of meso-N-TiO$_2$ deposited outside the silica template (after the removal of silica).
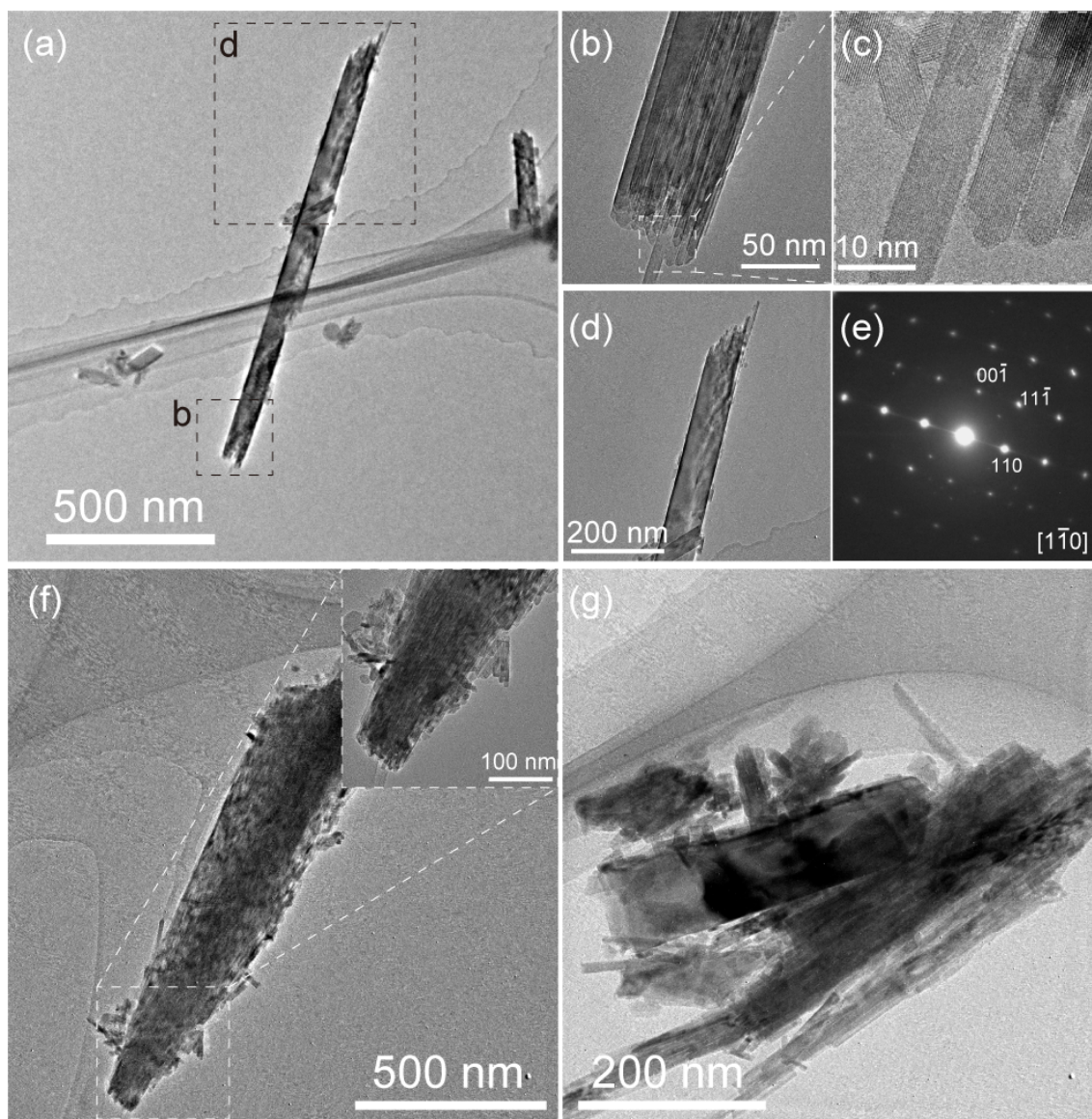
Fig. S14 (a) Low-magnification and (b), (c), and (d) high-magnification TEM images of template free-N-TiO₂. (e) SAED pattern of the whole particle observed in the TEM image of (a). (f) and (g) TEM images taken in the areas different from (a).

The lattice fringe forming parallel to the direction of the rod elongation was observed in Fig. S14(c). The lattice fringe spacing was 0.32 nm and it was assigned to the (110) plane of rutile TiO_2, indicating that the defects between the rods formed parallel to the rutile (110) plane. Therefore, the streaks found perpendicularly to the direction of the rod elongation (i.e. the spots observed in SAED pattern of Fig. S14(e)) are considered to be due to the defects between the rods forming parallel to the (110) plane.[1]
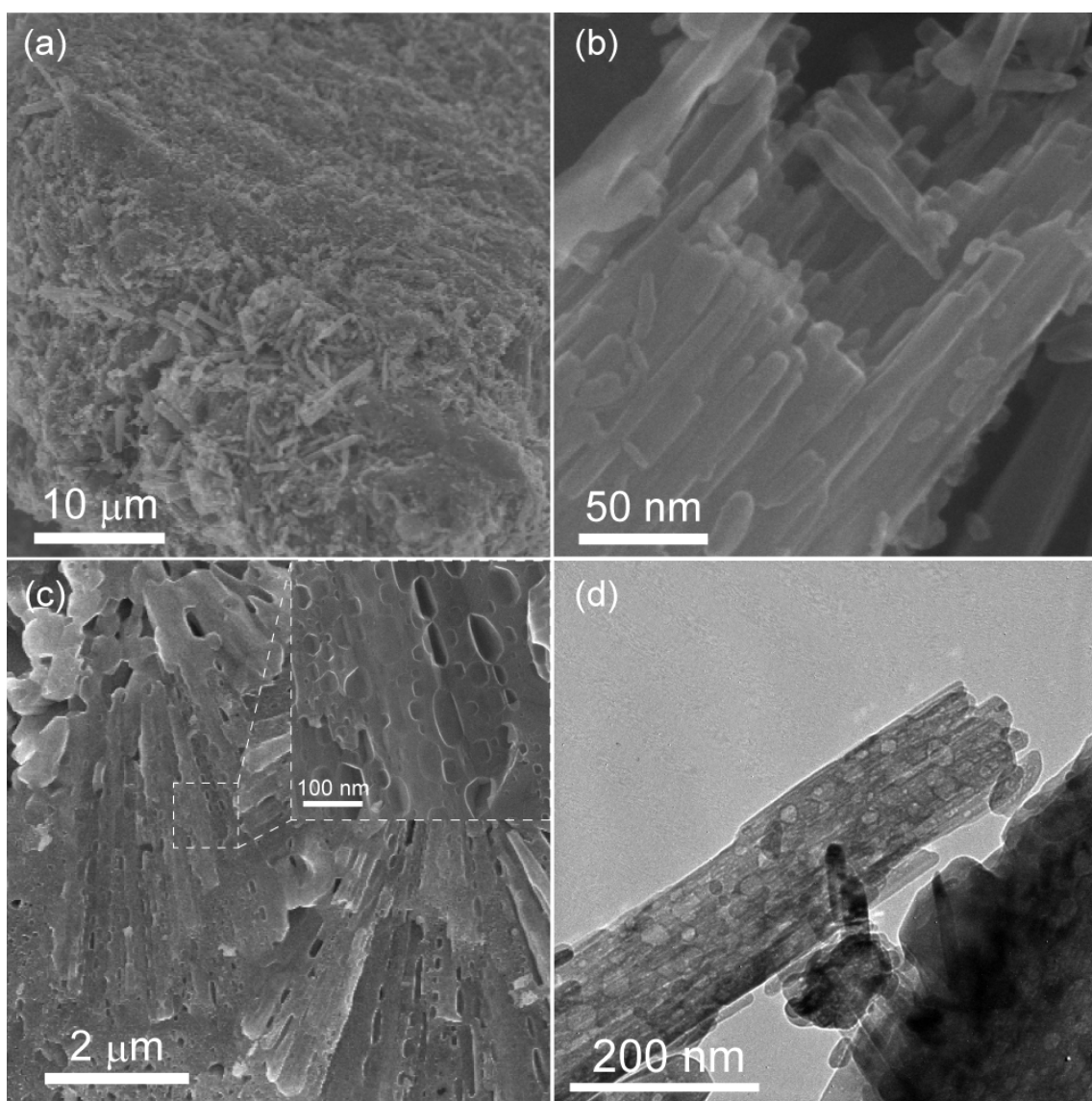
Fig. S15 (a) Low-magnification and (b), (c) high-magnification SEM images, and (d) TEM image of template free-N-TiO$_2$_873.
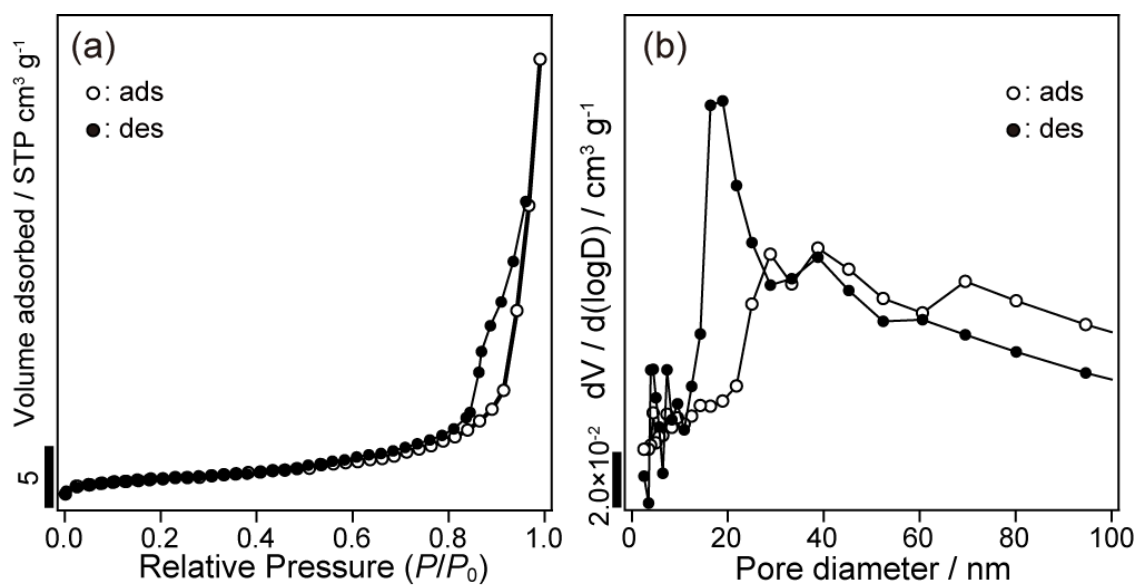
Fig. S16 (a) N_2 adsorption-desorption isotherms and (b) BJH pore size distributions of template free-N-TiO_2_873.
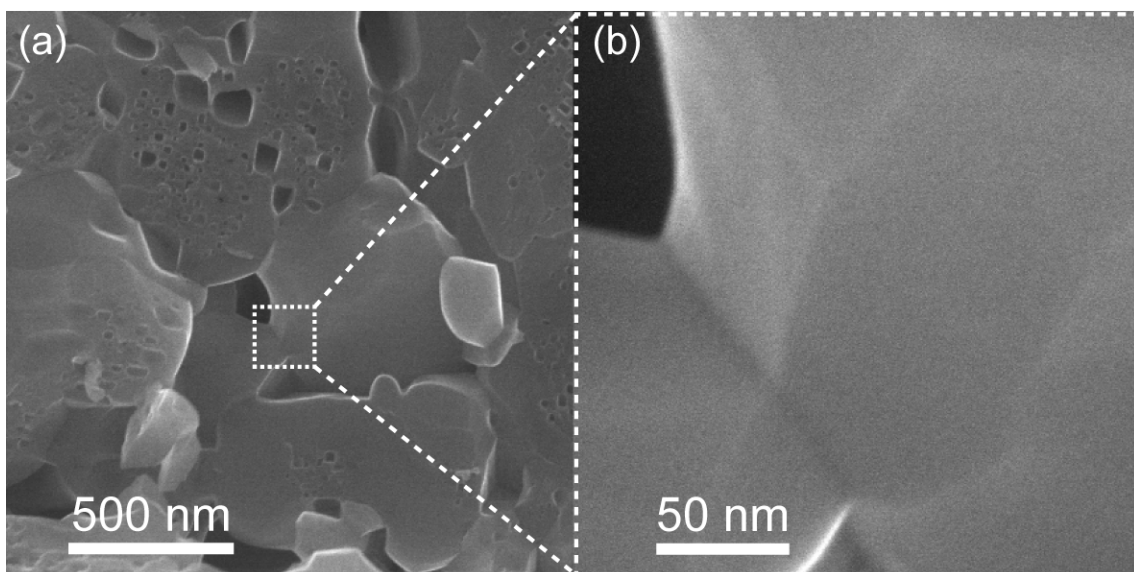
Fig. S17 (a) Low-magnification and (b) high-magnification SEM images of template free-N-TiO$_2$_1173.

Calculation of the pore volume in the sintered samples

1) Total pore volume

Using the formula (1) shown in the experimental section (main text), the densities of meso-N-TiO$_2$_873, template free-N-TiO$_2$_873, and template free-N-TiO$_2$_1173 were 2.48, 2.67, and 3.67 g cm^{-3}, respectively. The porosity of meso-N-TiO$_2$_873, template free-N-TiO$_2$_873, and template free-N-TiO$_2$_1173 calculated from the formula (2) shown in the experimental section were 0.42, 0.37, and 0.14, respectively. Therefore, the total pore volumes of these samples were calculated as follows.

meso-N-TiO$_2$_873:	0.42/2.48 g cm^{-3} = 1.69×10^{-1} cm^3 g^{-1}
template free -N-TiO$_2$_873:	0.37/2.67 g cm^{-3} = 1.39×10^{-1} cm^3 g^{-1}
template free -N-TiO$_2$_1173:	0.14/3.67 g cm^{-3} = 3.81×10^{-2} cm^3 g^{-1}

2) *Intra*particle pore volume

Based on the N$_2$ adsorption-desorption measurements, the *intra*particle pore volume of meso-N-TiO$_2$_873 and template free-N-TiO$_2$_873 were obtained as follows. Relative pressures up to 0.99 were used in the calculation of *intra*particle pore volumes. This is because, in general, the N$_2$ adsorption volume up to a relative pressure of 0.99 corresponds to the N$_2$ adsorption volume in pores with a pore size of about 200 nm or less, calculated from the Kelvin equation.[2]

meso-N-TiO$_2$_873:	1.0×10^{-1} cm^3 g^{-1}
template free -N-TiO$_2$_873:	6.3×10^{-2} cm^3 g^{-1}

For template free-N-TiO$_2$_1173, N$_2$ adsorption-desorption isotherms were not recorded because there were few *intra*particle pores.

3) *Inter*particle pore volume

*Inter*particle pore volumes of meso-N-TiO$_2$_873, template free-N-TiO$_2$_873, and template free-N-TiO$_2$_1173 were calculated as the following formula.

*inter*particle pore volume = total pore volume − *intra*particle pore volume

The calculated values of these samples show as follows.

meso-N-TiO$_2$_873:	6.9×10^{-2} cm^3 g^{-1}
template free -N-TiO$_2$_873:	7.6×10^{-2} cm^3 g^{-1}
template free -N-TiO$_2$_1173:	The value is same as the total pore volume.

Reasonability of the Eucken model for the estimation of the effect of *inter*particle pores on the reduction in the thermal conductivity

The presence of *inter*particle pores contributes to the reduction in the thermal conductivity by both radiation and convection through the pores.[3] The SEM images of meso -N-TiO$_2$_873 (Fig. 5a), template free-N-TiO$_2$_873 (Fig. S15a), and template free-N-TiO$_2$_1173 (Fig. S17a) show that the presence of the *inter*particle pores in a sub-micrometer size. The degree of reduction in the thermal conductivity due to those pores can be estimated by the Eucken model,[4] as explained below. The estimation should be ideally carried out using the Monte Carlo ray tracing simulation.[5] The values calculated by the Eucken model and those by the simulation for the estimation of the degree of reduction in the thermal conductivity due to pores in a sub-micrometer are reported to be virtually consistent with each other.[6] Therefore, the Eucken model was used to estimate the degree of thermal conductivity.

Contribution of the coherent and incoherent phonons to the reduction of the thermal conductivity in the nanoporous structures of meso-N-TiO$_2$_873 and template free-N-TiO$_2$_873

In nanoporous materials with different pore shapes, coherent and incoherent phonons have been discussed as factors that cause different degrees of reduction in thermal conductivity. The difference in thermal conductivities between meso-N-TiO$_2$_873 and template free-N-TiO$_2$_873 is considered to be attributed to incoherent phonons by the following discussion.

J.-K. Yu *et al.* reported that the thermal conductivity of nanomeshes (single crystal Si thin film with rectangular arrangement of 11 nm pores with 23 nm intervals) was about 88% lower than that of single crystal Si thin film.[7] They also reported that the thermal conductivity of single crystal Si nanowires with a width of 28 nm was 79% lower than that of single crystal Si thin films. They claimed that this difference in the reduction in the thermal conductivity is attributed to the coherent interference based on the wave nature of phonons in the nanomeshes with pore regularity.

In contrast to the preceding argument, N. K. Ravichandran *et al.* interpreted differently by their simulation results using the Boltzmann transport equation based on the phonon transfer as incoherent particles nature.[8] They concluded that the lower thermal conductivity of nanomeshes compared to nanowires is attributed to the higher fraction of backscattering of phonons at the pore wall surfaces. According to their simulation result, the wall surfaces of the nanowires were aligned parallel to the direction of heat transfer (temperature gradient) and 50% of the incident phonons are backscattered on average. On the other hand, the pore wall surfaces of the nanomeshes were not parallel to the direction of heat transfer and approximately 70% of the incident phonons are backscattered. Because the backscattering of phonons reduces the contribution of the phonon conduction to heat transfer, the thermal conductivity of the nanomeshes was further reduced. J. Lee *et al.* also support the effect of the phonon backscattering by their experimental and simulated results.[9] They measured the thermal conductivities of nanomeshes with different pitches between pore wall surfaces, and the thermal conductivity of the nanomeshes with a shorter pitch was lower. This was because there are more pore wall surfaces introducing the backscattering of phonons in the nanomeshes with a shorter pitch. This result was in good agreement with the values of thermal conductivities calculated from the Boltzmann transport equation.

It is known that the coherent interference is observed only at cryogenic temperature in nanoporous structures with the pore size of tens to hundreds of nanometers.[10] In addition, it is predicted that the fabrication of nanostructures with pores and periodicity smaller

than tens of nanometers is necessary to observe the coherent interference at room temperature. Therefore, the difference in thermal conductivities between meso-N-TiO$_2$_873 and template free-N-TiO$_2$_873 is considered to be attributable to the higher fraction of backscattering of phonons for meso-N-TiO$_2$_873.
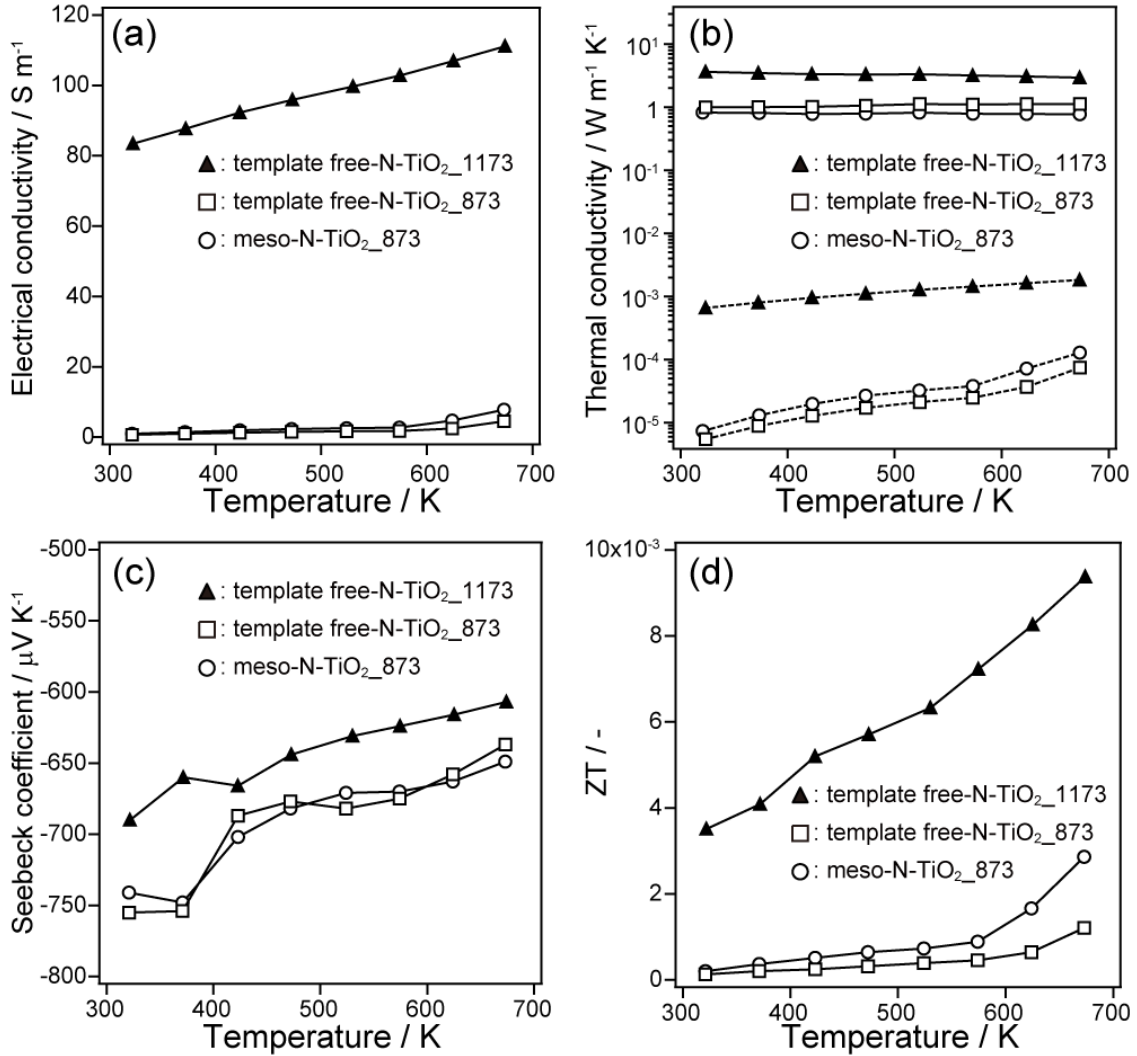
Fig. S18 (a) Electrical conductivities, (b) thermal conductivities (solid line: measured thermal conductivities, dotted line: carrier thermal conductivities calculated from the Wiedemann-Frantz law), (c) Seebeck coefficients, and (d) ZT values of meso-N-TiO$_2$_873, template free-N-TiO$_2$_873, and template free-N-TiO$_2$_1173.

The values of σ and S of meso-N-TiO$_2$_873, which are related to carrier transport, were almost the same as those of template free-N-TiO$_2$_873 prepared without silica. These results suggest that the residual silica did not affect the electrical properties in the interfaces between TiO$_2$ particles. Phonons, which mainly transport through the pore walls of TiO$_2$, may be scattered at the interfaces between TiO$_2$ particles due to the residual silica, but the residual silica is so slight that it has little effect on carrier transport, ensuring carrier paths. Therefore, it is considered that the residual silica did not affect the κ either.

References

1. A. Wisnet, S. B. Betzler, R. V. Zucker, J. A. Dorman, P. Wagatha, S. Matich, E. Okunishi, L. Schmidt-Mende and C. Scheu, *Cryst. Growth Des.*, 2014, **14**, 4658–4663.
2. K. L. Murray, N. A. Seaton and M. A. Day, *Langmuir*, 1999, **15**, 6728–6737.
3. A. L. Loeb, *J. Am. Ceram. Soc.*, 1954, **37**, 96–99.
4. A. Eucken, *Forsch. Ing.-Wes.*, 1940, **11**, 6–20.
5. T. Hori, J. Shiomi and C. Dames, *Appl. Phys. Lett.*, 2015, **106**, 171901.
6. M. Kashiwagi, Y. Sudo, T. Shiga and J. Shiomi, *Phys. Rev. Appl.*, 2018, **10**, 044018.
7. J. K. Yu, S. Mitrovic, D. Tham, J. Varghese and J. R. Heath, *Nat. Nanotechnol.*, 2010, **5**, 718–721.
8. N. K. Ravichandran and A. J. Minnich, *Phys. Rev. B*, 2014, **89**, 205432.
9. J. Lee, W. Lee, G. Wehmeyer, S. Dhuey, D. L. Olynick, S. Cabrini, C. Dames, J. J. Urban and P. Yang, *Nat. Commun.*, 2017, **8**, 14054.
10. J. Maire, R. Anufriev, R. Yanagisawa, A. Ramiere, S. Volz and M. Nomura, *Sci. Adv.*, 2017, **3**, e1700027.